Critical Fluctuations in Liquid-Liquid Extraction Organic Phases Controlled by Extractant and Diluent Molecular Structure

Brittany L. Bonnett,[†] Dina Sheyfer,[‡] Pubudu N. Wimalasiri,[†] Srikanth Nayak,[†] Jyotsana Lal,[¶,§] Qingteng Zhang,[‡] Soenke Seifert,[‡] G. Brian Stephenson,[*,¶] and Michael J. Servis[*,†]

[†]*Chemical Sciences and Engineering Division, Argonne National Laboratory, Lemont, IL 60439, USA*

[‡]*X-ray Science Division, Argonne National Laboratory, Lemont, IL 60439, USA*

[¶]*Materials Science Division, Argonne National Laboratory, Lemont, IL 60439, USA*

[§]*Department of Physics, Northern Illinois University, DeKalb, IL 60115, USA*

E-mail: gbs@anl.gov; mservis@anl.gov

Abstract

Extractant aggregation in liquid-liquid extraction organic phases impacts extraction energetics and is related to the deleterious efficiency-limiting liquid-liquid phase transition known as third phase formation. Using small angle x-ray scattering, we find that structural heterogeneities across a wide range of compositions in binary mixtures of malonamide extractants and alkane diluents are well described by Ornstein-Zernike scattering. This suggests that structure in these simplified organic phases originates from the critical point associated with the liquid-liquid phase transition. To confirm this, we measure the temperature dependence of the organic phase structure, finding critical exponents consistent with the 3D Ising model. Molecular dynamics simulations were also consistent with this mechanism for extractant aggregation. Due to the absence of water or any other polar solutes required to form reverse-micellar-like nanostructures, these fluctuations are inherent to the binary extractant/diluent mixture. Our previous work found pseudobinary critical fluctuations near the critical point for more complex organic phases with extracted polar solutes, including water, acid and metal ions. Taken together, these results suggest this mechanism for explaining organic phase aggregation may dominate over a wide range of conditions encountered in practical liquid-liquid extraction organic phases. We also show how the molecular structure of the extractant and diluent modulate these critical concentration fluctuations by shifting the critical temperature: critical fluctuations are suppressed by increasing extractant alkyl tail lengths or decreasing diluent alkyl chain lengths. This is consistent with how extractant and diluent molecular structure are known to impact metal and acid loading capacity in many-component LLE organic phases, suggesting phase behavior of practical systems may be effectively studied in simplified organic phases. Overall, the explicit connection between molecular structure, aggregation and phase behavior demonstrated here will enable the design of more efficient separations processes.

Introduction

The selective recovery of critical materials, including metals, enables a wide range of important technologies.[1,2] Owing to its scalability and low input energy requirements, liquid-liquid extraction (LLE) is a predominant method for separations of metals, including rare earth elements,[3–9] actinides,[10,11] and platinum group elements.[12] In LLE, amphiphilic extractant molecules bind metals, transferring them from a polar aqueous phase to an immiscible nonpolar organic phase.[13] The distribution of metals between the two phases depends on the difference in solvation free energy between those phases. As the energy difference needed for effective, reversible separations processes can be relatively small, even as small as the thermal energy, a frontier of separations research is understanding the impact of organic phase structure beyond the primary metal coordination sphere.[7,14–18] To that end, LLE systems are often modeled as microemulsions, where organic phase structure is treated as colloidal particles representing reverse micellar aggregates.[19–43]

An important limitation of LLE is third phase formation,[28,44] a liquid-liquid phase transition where, upon sufficient loading of polar solutes into the nonpolar organic phase, it splits into "heavy" and "light" phases. The heavy phase contains most of the extractant molecules and extracted polar species, while the light phase primarily consists of the organic solvent, also called the diluent.[45] The resulting three-phase system is incompatible with processing equipment, resulting in a limit to the per-contact loading capacity of the organic phase. While organic phase structure has long been linked to its phase behavior,[20,39,43,46–58] we recently proposed that organic phase structure over a wide range of binary extractant/diluent mixtures is consistent with critical fluctuations originating from the critical point associated with the third phase formation phase transition.[59,60] This could explain certain limitations to common microemulsion descriptions of LLE systems, such as the presence of structure in the organic phase even in the absence of extracted polar solutes needed to induce the formation of water-in-oil aggregates.[61]

Our recent studies find that the fluctuations in many-component organic phases contain-

ing extracted acid, water and metal salts are quantitatively consistent with the theory of critical phenomena.[62] In particular, the scattering obeys an Ornstein-Zernike relation typical of critical fluctuations, with divergent behavior as the critical temperature for phase separation is approached that agrees with predictions for the 3D Ising model.[63,64] Since this universality class of phase transitions includes binary fluid mixtures, this indicates that pseudobinary critical fluctuations develop along a single compositional degree of freedom. This suggests that the theory of critical phenomena may provide a deep, quantitative connection between structure and phase behavior in LLE that can be meaningfully explored through simplified organic phases. To test this applicability of simplified organic phases to complex, realistic LLE organic phases, we investigate critical scaling through temperature dependence of organic phase structure in binary extractant/diluent mixtures, which allows us to compare critical behavior to more complex organic phases. We look to see if well-known relationships between extractant and diluent alkyl chain lengths and their impact on promoting or inhibiting third phase formation[44,65–68] can be reproduced in these simplified systems. If this were the case, it might suggest that screening of compatible extractant/diluent combinations can be conducted in simplified systems that are easier to study experimentally and computationally.

In this study, we explore the role of extractant and diluent molecular structure on organic phase aggregation in binary mixtures of extractant and diluent. (Here, we define compositions by the extractant volume fraction, φ_E.) We consider linear alkane diluents with a family of malonamide extractants, shown in Figure 1, which are commonly applied to lanthanide separations.[69–71] We use small angle x-ray scattering (SAXS) to quantify the concentration fluctuations associated with the phase instability over the full range of extractant/diluent compositions, for diluents and extractants of various molecular lengths. For the organic phase having a critical temperature, T_C, closest to room temperature, we measure temperature-dependent SAXS patterns to obtain critical exponents. Then, we investigate this mechanism of organic phase aggregation with molecular dynamics (MD) simulations.

Our findings suggest that critical fluctuations could be responsible for the widely reported nanostructuring found in a wide range of LLE organic phases.

Methodology

Sample Preparation

Purified extractants *N*,*N*'-dimethyl,*N*,*N*'-dibutyltetradecylmalonamide (DMDBTDMA, > 99% purity by HPLC) and *N*,*N*'-dimethyl,*N*,*N*'-dibutylpentylmalonamide (DMDBPMA, > 98% purity by HPLC) were purchased from Technocomm Ltd and *n*-alkanes were purchased from Sigma-Aldrich (> 99% purity). All reagents were used as-received. Samples for each composition were prepared by massing extractant (density of DMDBTDMA = 0.908 g/cm^3; density of DMDBPMA = 0.935 g/cm^3) followed by volumetric dilution with the corresponding diluent. Volume fractions and concentrations of each sample are given in Table S1.

SAXS Experiments

SAXS measurements at fixed temperature, 298 K (25° C), were conducted at beamline 12-ID-C[72] at the Advanced Photon Source (APS). Samples were loaded into a 2-mm-outer-diameter quartz capillary. Data was collected from a Pilatus 2M detector using a 2.133 m sample-to-detector distance with an 18 keV incident energy. Scattering patterns were normalized to an absolute scale after empty capillary subtraction using scattering from pure water.[73] All SAXS patterns were averaged over five one-second exposures. Variable temperature SAXS measurements were conducted at beamline 8-ID-I at the APS, with experimental details the same as those described by Sheyfer et al.[64] Sample temperature was stepped in 0.2 K increments and monitored to 0.1 K accuracy with type K thermocouples.

Molecular Dynamics Simulations

The simulation force field details and methodology are the same as we previously reported.[59] Simulation compositions are reported in Table S2. Simulations were conducted with the GROMACS 2016.2 software package.[74] Force field details for DMDBPMA and dodecane are reported in Ref. 61. Initial configurations were created with Packmol,[75] followed by energy minimization using a steepest descent algorithm. Each simulation was equilibrated for 5 ns in the NPT ensemble, followed by 20 ns of equilibration in the NVT ensemble and 50 ns of production in the NVT ensemble. In the NPT ensemble, pressure was set to 1 bar with the Berendsen barostat[76] using a 2 ps coupling time and temperature was set to 300 K using a 0.2 ps coupling time with the velocity rescale thermostat.[76] In the NVT ensemble, temperature was set to 300 K with the Nosé-Hoover thermostat[77] with a 0.2 ps coupling time. Dynamics were conducted using a 2 fs time step using the leap-frog Verlet integrator,[78] with hydrogen-containing bonds constrained using the LINCS algorithm.[79] A 15 Å cutoff was used for Lennard-Jones and short-range electrostatic interactions, with particle-mesh Ewald summation used for long-range electrostatics.[80] Trajectories were sampled for analysis at 100 ps intervals.

Results

Phase Behavior and Effect of Extractant and Diluent Chain Lengths

Practical LLE systems contain an aqueous and organic phase where, after splitting, the dense organic phase is referred to as the third phase. In this study we consider just the organic phase such that the associated phase transition is from one phase to two. Third phase formation is widely associated with organic phase separation upon cooling;[60,63–65,81] Figure 1A shows the T-φ_E diagram with this upper critical solution temperature (UCST) behavior. We consider two extractants: DMDBTDMA and DMDBPMA, shown in Figure

1. The former is commonly applied to rare earth separations while the latter is a more hydrophilic analog that has been used to investigate the role of extractant lipophilicity.[59,82,83] As illustrated in the schematic phase diagrams in Figure 1B, organic phase mixtures are prepared with φ_E increments of 0.10 for combinations of DMDBPMA with hexane, octane, decane, dodecane and hexadecane, and DMDBTDMA mixtures are prepared with dodecane. While the critical temperature for DMDBPMA/hexadecane is measured in the following section, the shape of the coexistence curve and relative location for each mixture are only intended to be schematic and are inferred from the strength of the concentration fluctuations measured at room temperature, as discussed below.

Organic phase structure across the phase diagram is quantified to understand the extent of critical fluctuations in these systems. For aggregation driven by such fluctuations, we expect increased lengthscales associated with compositions near the critical point. Scattering data for the DMDBPMA systems are plotted in Figure 2, and data for DMDBTDMA in Figure 3. Using the Ornstein-Zernike equation,

$$I(Q) = \frac{I_{Q=0}}{1 + (\xi Q)^{2-\eta}} + B, \tag{1}$$

which describes scattering intensity, $I(Q)$, as a function of scattering wavevector, Q, resulting from critical fluctuations,[62] we $I_{Q=0}$, the correlation length, ξ, and background (noncritical) scattering, B, for each mixture. Fits are shown in Figures S1 and S2 for DMDBPMA and DMDBTDMA, respectively, with fitted values plotted in Figure S3. Here, we assume classical Ornstein-Zernike behavior, taking the Fisher dimensional anomaly exponent,[84,85] η, to be zero. In the following section, we fit η along with the other static critical exponents using temperature-dependent scattering data.

While the above approach provides good fits for many of our systems, the behavior of the fitted parameters are inconsistent at high values of φ_E, where the strength of the critical fluctuations are weakest, as shown in Figures S3. In particular, best-fit values of $I_{Q=0}$ can

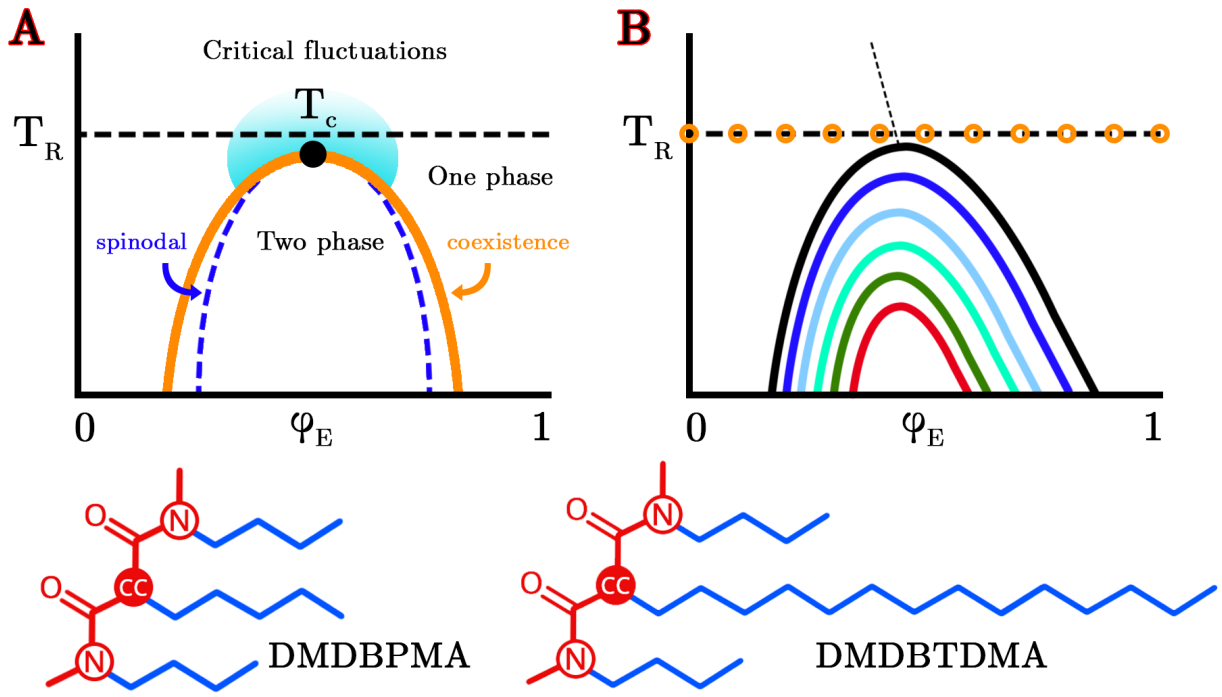

Figure 1: (A) A schematic phase diagram for these organic phases showing a typical upper critical solution temperature, with the region of critical fluctuations above the spinodal curve highlighted. (B) Schematic phase diagrams are shown for different binary mixtures considered in this study. The critical temperature, T_C, decreases with shorter diluent hydrocarbon chains and longer extractant chains: the black curve through the dark green curve in order of descending T_C corresponds to DMDBPMA mixtures with hexadecane, dodecane, decane, octane and hexane, respectively. The red curve corresponds to DMDBTDMA/dodecane. Orange open circles correspond to samples taken at room temperature (T_R) at various extractant volume fractions, φ_E. The Widom line (dashed) is also illustrated for one mixture. Below, the two malonamides of interest, DMDBPMA and DMDBTDMA, are shown with "central carbon" (CC) atoms highlighted.

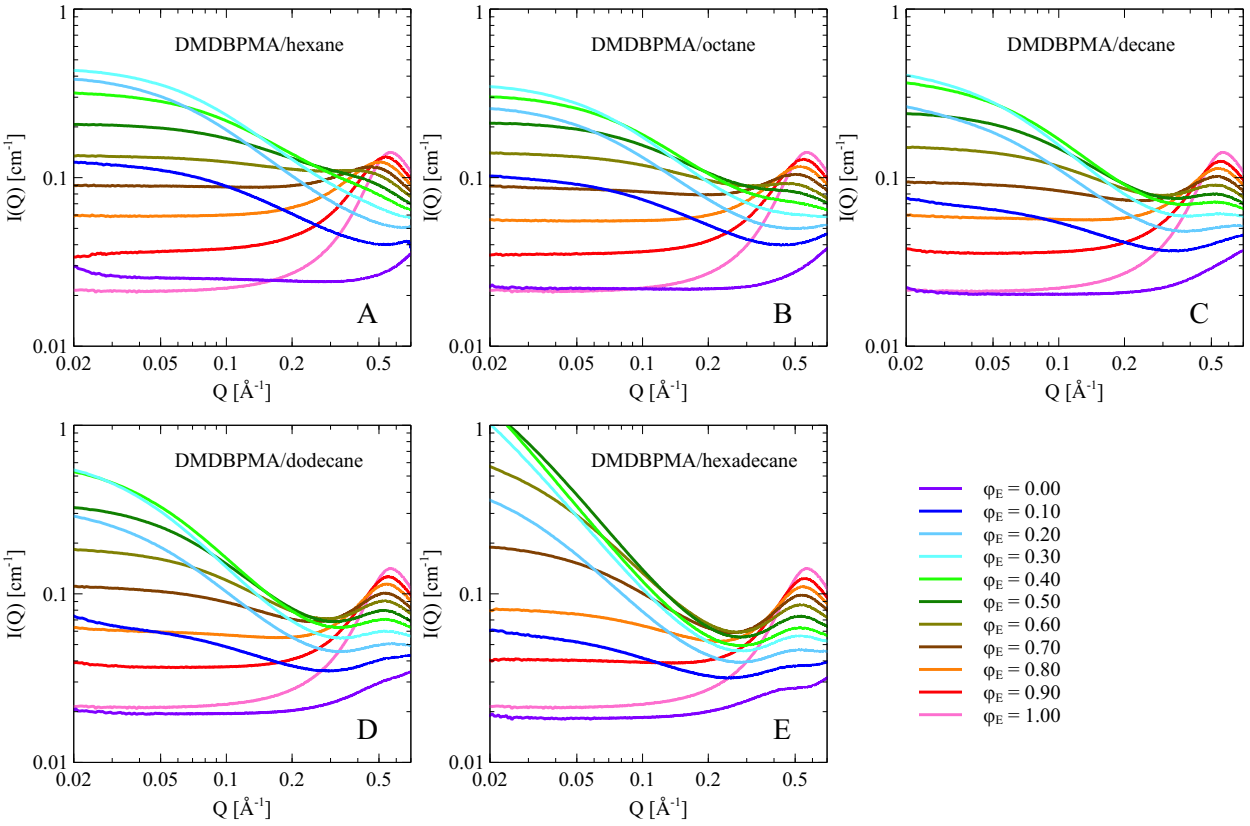

Figure 2: The SAXS patterns for each DMDBPMA mixture, defined by extractant volume fraction, φ_E, are shown in panels A-E for increasing diluent chain length from hexane to hexadecane.

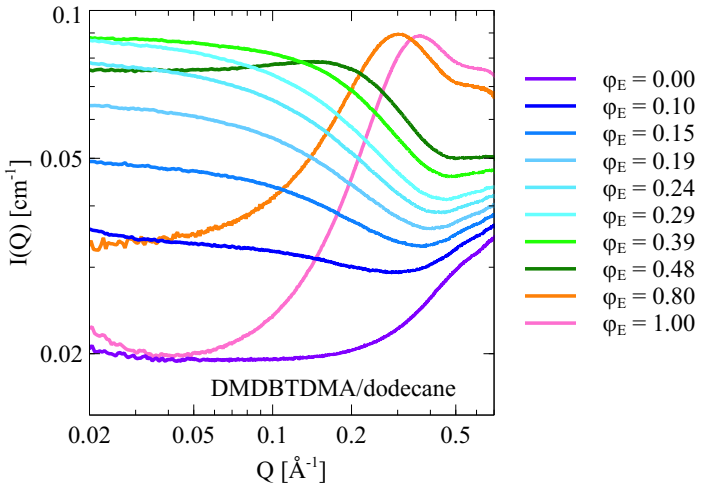

Figure 3: The SAXS patterns are plotted for each DMDBTDMA mixture with dodecane.

become negative and the fitted background scattering, B, increases with φ_E compared to the weighted average of the pure components. To address this, we instead fit $I(Q)_{\text{sub}}$ to the Ornstein-Zernike equation,

$$I(Q)_{sub} \equiv I(Q) - [\varphi_E I(Q)_{\text{ext}} + (1-\varphi_E) I(Q)_{\text{dil}}] = \frac{I_{Q=0}}{1+(\xi Q)^2}, \tag{2}$$

where we have subtracted the weighted average of the scattering of the pure extractant and diluent, $I(Q)_{\text{ext}}$ and $I(Q)_{\text{dil}}$, respectively, from $I(Q)$. By subtracting the pure component scattering patterns, the remaining scattering results from the structural correlations present in the solution: in this case, the structure factor associated with the concentration fluctuations. The Ornstein-Zernike fits to $I(Q)_{\text{sub}}$ are shown in Figures S4 and S5 for DMDBPMA and DMDBTDMA, respectively, with comparisons of the fitted ξ and $I_{Q=0}$ values from $I(Q)$ and $I(Q)_{\text{sub}}$ in Figure S3. Comparing the trends with φ_E for these two fitting approaches, it is clear that we obtain better fits after subtracting the weighted average of the pure components. At middling extractant volume fractions where the fluctuations are strongest, the trends in ξ and $I_{Q=0}$ are the same, with larger absolute values using $I(Q)$. At low and high φ_E where the Ornstein-Zernike scattering is relatively small and harder to accurately fit or, in the case of DMDBTDMA, is disrupted by the pre-peak characteristic of the pure extractant SAXS pattern, subtracting the pure component scattering patterns provides a significant improvement to the fitting. Therefore, we proceed with our analyses using this approach.

Overall, we find the low-Q region of $I(Q)_{\text{sub}}$ in all of the mixtures for each extractant and diluent pair are described well by the Ornstein-Zernike equation. The fitted values of ξ and $I_{Q=0}$ are shown in Figure 4A-B for each system. In each binary mixture, these properties exhibit maxima near $\varphi_E = 0.20 - 0.40$. This behavior is consistent with the compositional isotherm for $T > T_C$ crossing the Widom line in the single-phase region. The Widom line, illustrated in Figure 1B, is defined as the locus of correlation length maxima extending from

the critical point into the single phase region.[86–92] Along the critical isotherm, $T = T_C$, the correlation length diverges at the critical composition; for $T > T_C$, it instead reaches a maximum at the Widom line with the strength of this maximum increasing as T approaches T_C (see discussion of temperature scaling in the following section). The Widom line is often conceptualized as demarcating the transition between low- and high-density-like mixtures, such as liquid-like and gas-like regions above T_C for a liquid-vapor critical point,[89,92] or low- and high-density-like water mixtures above the liquid-liquid critical point in supercooled water.[86,88,90] For the liquid-liquid critical point associated with third phase formation, the low-density compositions corresponds to extractant clustering within the nonpolar alkane diluent, while the high-density corresponds to the inverse case. While there is no thermodynamic phase transition separating extractant-in-diluent mixtures from diluent-in-extractant, the location of the Widom line at a given T represents the composition at which the two components are most strongly interspersed.

The molecular structure of the extractant and diluent strongly affects the critical fluctuations at room temperature, both in magnitude and the location of the Widom line. Figure 4 shows how decreasing diluent chain length reduces the strength of fluctuations. This occurs because the shorter diluents reduce T_C, which is consistent with how shorter alkane diluents are widely understood to promote inhibit third phase formation.[44,65–68] The fact that trends in third phase formation are consistent with trends in concentration fluctuations of the binary mixture suggests a similar mechanism of extractant/diluent compatibility in both cases. The description of shorter alkane diluents better wetting or solubilizing the metal-extractant complexes/reverse micelles, inhibiting their self-association, is consistent with the reduced concentration fluctuations we observe in simplified binary organic phases. Interestingly, some compositions of the DMDBPMA/hexane mixture have larger values of $I_{Q=0}$ (but not ξ) than longer alkanes. This can be attributed to the larger density difference between shorter alkane diluents and the extractant than for longer alkanes (DMDBPMA has a mass density of 0.935 g/cm^3 compared to 0.750 g/cm^3 for dodecane and 0.655 g/cm^3 for

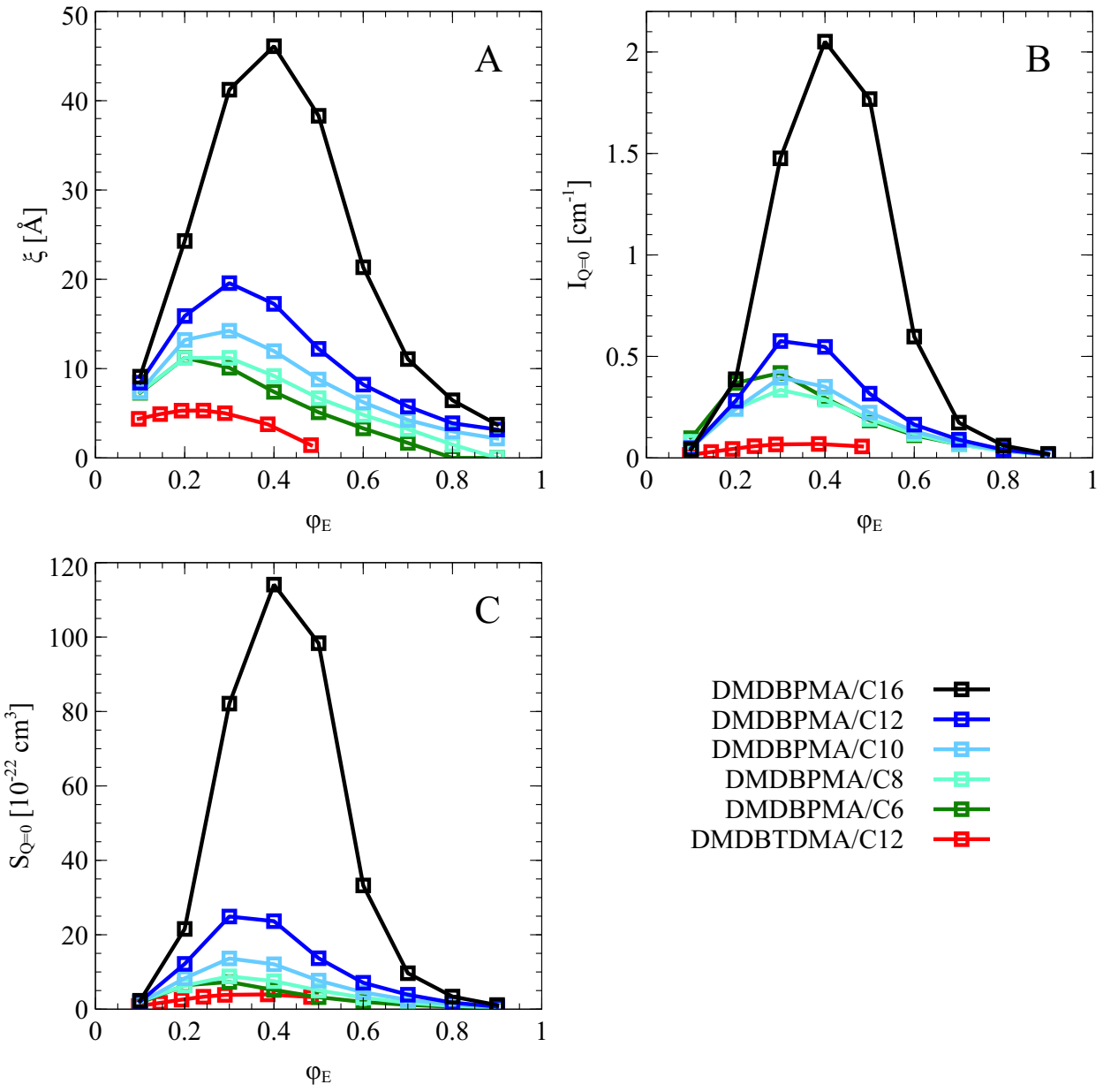

Figure 4: The fitted ξ (A), $I_{Q=0}$ (B) and $S_{Q=0}$ (C) values are plotted for each binary mixture.

hexane[93]), which contributes to $I_{Q=0}$ but not ξ.[94,95] Decreasing diluent chain length reduces the correlation length of fluctuations less and less at smaller chain lengths, but the decrease in diluent density remains roughly linear with chain length. Therefore, the contribution to $I_{Q=0}$ from the increasing difference in density between the two components out-competes the decrease in concentration fluctuations at sufficiently low diluent chain length. We account for this by converting $I_{Q=0}$ to a structure factor using

$$S_{Q=0} = \frac{I_{Q=0}}{r_e^2(\rho_{e,ext} - \rho_{e,dil})^2}, \tag{3}$$

where $\rho_{e,ext}$ and $\rho_{e,dil}$ are the electron densities of the extractant and diluent, respectively, and r_e^2 is the Thomson scattering length.[96] The relationship between $S_{Q=0}$ and composition is plotted for each system in Figure 4C, demonstrating that fluctuations decrease monotonically with decreasing diluent chain length.

We find that increasing the extractant chain length also reduces T_C, which is consistent with the widely reported impact of extractant chain length for malonamides[66] and other classes of extractant.[67] As with the role of diluent chain length above, this indicates the phase stability of simple binary mixtures can provide insight into more complex organic phases. However, another change in structure along the room temperature isotherm occurs as T_C is lowered: the correlation length maximum moves to lower extractant volume fractions. That is, more extractant is needed to maximize fluctuations the stronger those fluctuations are. This is attributed to the negative slope of the Widom line in the $\varphi_E - T$ phase diagram that is imparted by the asymmetry in the high- and low-density branches of the liquid-liquid coexistence curve. This impacts the slope of the line of rectilinear diameters, which the Widom line tracks into the single phase region.[92,97,98]

Temperature Scaling and Critical Exponents

To definitively demonstrate that the structural heterogeneities observed from small angle scattering are dominated by critical fluctuations—and to measure the associated critical exponents—we investigate the temperature scaling of the extractant/diluent mixture having its critical point closest to room temperature. For this mixture, DMDBPMA and hexadecane, we select the composition with the strongest room-T critical fluctuations: $\varphi_E = 0.40$. We measure the scattering at low Q while lowering T toward T_C. In this regime, we can fit the data with Eq. 1 with $B = 0$. From critical point theory, the temperature scaling of ξ and $I_{Q=0}$ are expected to follow power laws given by

$$\xi(\epsilon) = \xi_0 \epsilon^{-\nu} \tag{4}$$

and

$$I_{Q=0}(\epsilon) = I_0 \epsilon^{-\gamma}. \tag{5}$$

Here, ϵ is the reduced temperature, defined as

$$\epsilon \equiv (T - T_{sp})/T_{sp}, \tag{6}$$

where T_{sp} is the spinodal temperature, which is equal to T_C at the critical composition. The critical exponents, γ and ν, and the Fisher dimensional anomaly exponent are expected to be related through[84,85]

$$\gamma = \nu(2 - \eta). \tag{7}$$

As shown in Fig. 5A, the scattering patterns for this mixture show increased critical fluctuations with decreasing temperature, as expected for UCST behavior. Also shown is a simultaneous fit of the scattering at all temperatures using independent values of ξ and $I_{Q=0}$ at each T, but a single value of η, as done previously in Ref. 64. Using these values, all curves collapse onto a single master curve, Fig. 5B. Values of exponents γ and η and the

associated T_{sp} are obtained from fits shown in Fig. 6A and reported in Table 1. The fitted critical exponents are consistent with the 3D Ising model, having reported values of $\nu = 0.63$ and $\gamma = 1.24$.[99] The temperature scaling observed here is the same as we previously reported for complex, five-component malonamide/dodecane organic phases.[64] This highlights the universality of critical phenomena in its ability to describe a wide range of LLE organic phases, even when the nature of the aggregation is driven by different types of intermolecular interactions, i.e., amphiphile self-association versus clustering of extractant-metal complexes.

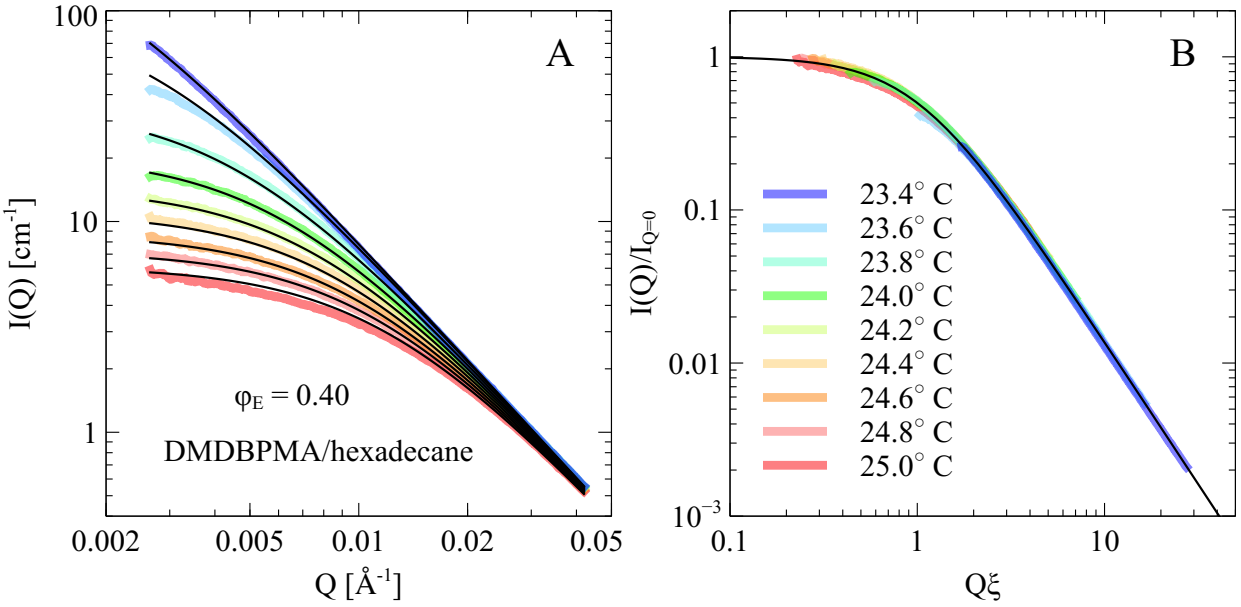

Figure 5: SAXS patterns (A) and master curve (B) for the $\varphi_E = 0.40$ DMDBPMA/hexadecane mixture is shown for each temperature.

Aggregation from Molecular Dynamics Simulations

Molecular simulation can provide a real-space description of solution structure, revealing the microscopic origins of aggregation. Figure 7A illustrates the nanoscale heterogeneities in extractant concentration that are evident from visual inspection of the simulation trajectories. In our previous Letter,[59] we quantified extractant clustering from simulation in this system, discussing the relative locations of the percolation and Widom lines and qualitatively

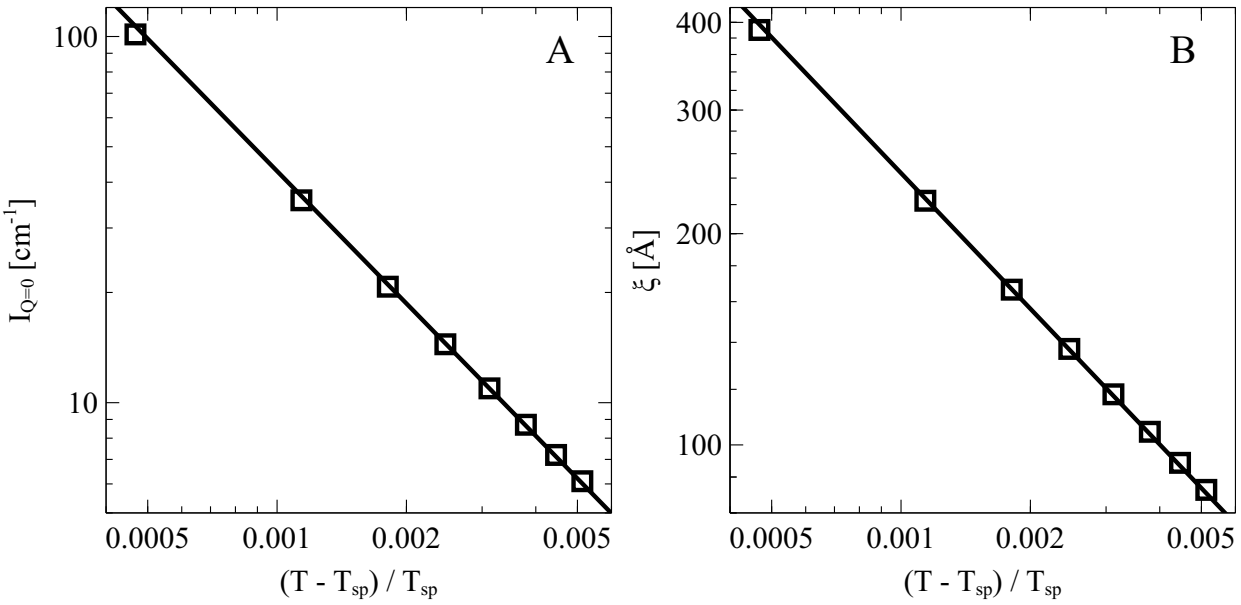

Figure 6: Power law fits of temperature scaling for the $\varphi_E = 0.40$ DMDBPMA/hexadecane mixture are shown for $I_{Q=0}$ (A) and ξ (B).

Table 1: Fitted parameters and critical exponents from DMDBPMA/hexadecane mixture for $\varphi_E = 0.40$.

Fisher exponent η	0.13 ± 0.01
Critical exponent ν	0.64 ± 0.02
Critical exponent γ	1.20 ± 0.04
$(2-\eta)\nu$	1.20
Correlation ampl. ξ_0 [Å]	2.89 ± 0.34
Scattering ampl. I_0 [cm^{-1}]	0.0107 ± 0.0027
$T_{\rm sp}$ from ξ [K]	296.63 ± 0.01
$T_{\rm sp}$ from $I_{Q=0}$ [K]	296.63 ± 0.01

comparing extractant cluster size distributions to the 3D Ising model. Here, we select four simulation compositions from the data reported in that study for DMDBPMA/dodecane mixtures to describe extractant aggregation under different conditions with increasing φ_E: below the percolation threshold, at the percolation threshold, above the percolation threshold, and for pure DMDBPMA.

Extractant aggregation is quantified by using both geometric and thermodynamic descriptions. For the geometric description, a graph-theoretic cluster analysis is performed on the extractant molecules[59,61,100] using the position of the carbon connecting the two amide groups and a distance cutoff of 10 Å, taken from the first minimum in the radial distribution function (RDF) for pairs of that atom type (see Figure 7). At low φ_E ($\varphi_E = 0.08$), we find that the cluster sizes are exponentially distributed. At $\varphi_E = 0.18$, the distribution is a power law with exponent consistent with the percolation critical exponent for cluster size in three dimensions, $\tau = 2.19$.[101] Then, at higher φ_E, a spanning cluster exists in dynamic equilibrium with exponentially distributed clusters of finite size. Lastly, with $\varphi_E = 1.00$, there is a single spanning cluster. Overall, these broad distributions of cluster sizes indicate that extractant self-association does not feature characteristic aggregate sizes in any concentration regime. Monodisperse particle models, such as the spherical tetramers or larger rod-like reverse micelles[82] that have been proposed in the literature are, therefore, not necessarily appropriate for organic phases dominated by critical concentration fluctuations of the binary extractant/diluent mixture. The temperature dependence of scattering patterns or other measures of particle size, such as diffusivity,[36] may assist differentiation of structure factor and particle factor contributions to scattering. As we previously noted,[59] geometric and thermodynamic descriptions of solution structure are not identical and the divergence of the mean cluster size and the maximum of the Ornstein-Zernike correlation length do not generally coincide.[59,92,102] For a second approach to quantifying solution structure, next we directly measure the thermodynamic concentration fluctuations observed from the simulations.

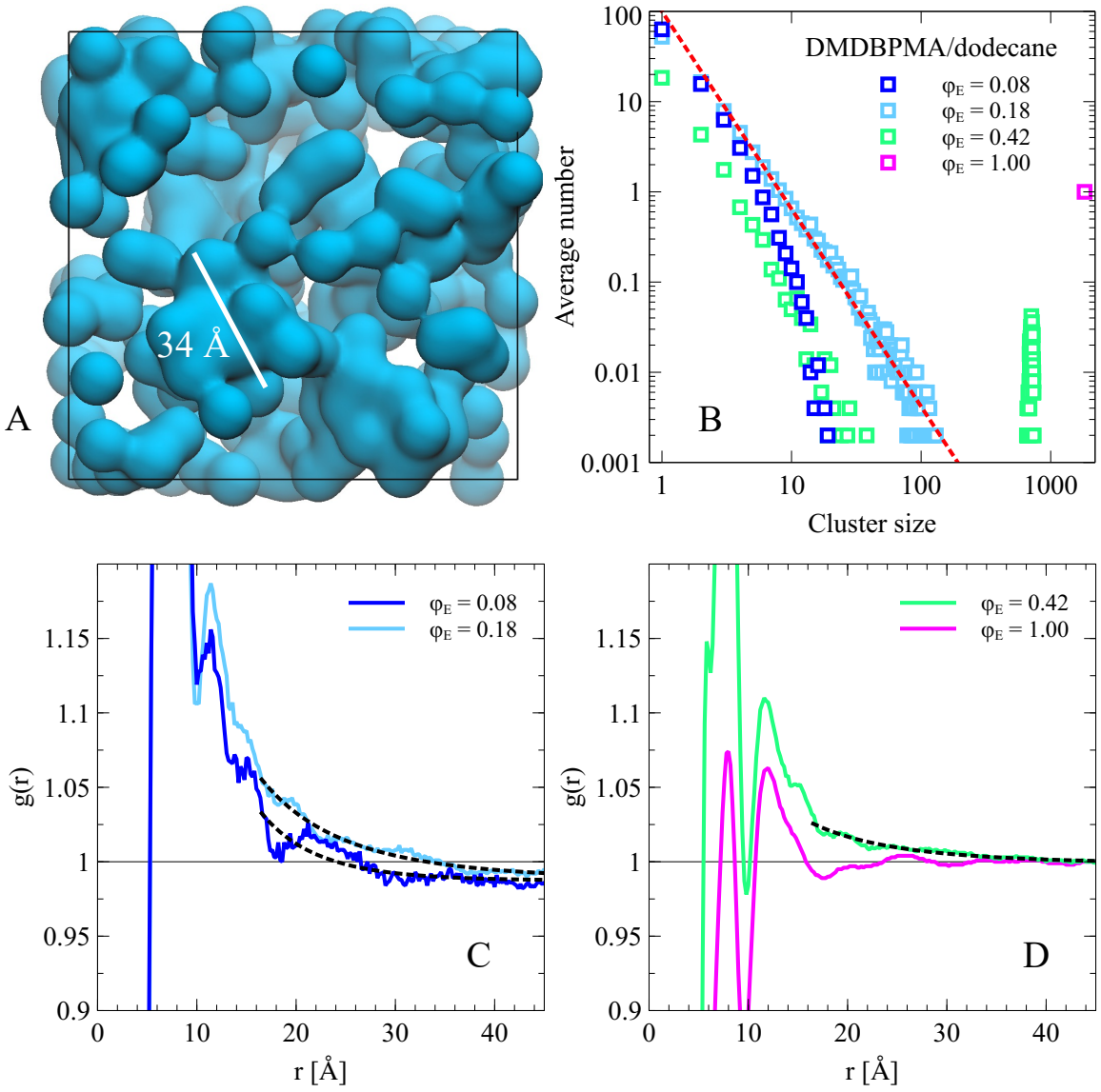

Figure 7: Panel A shows a snapshot from the $\varphi_E = 0.18$ DMDBPMA/dodecane mixture with a surface representation of the extractant molecules using the positions of the "CC" amide-bridging carbon atoms. Diluent is omitted for clarity. Panel B shows the extractant cluster size distributions for each of the four simulations. The red dashed line is the power law distribution for cluster sizes in three dimensions from percolation theory. Panels C and D show the CC-CC RDFs for each simulation, with fits to the long-range decay using the experimental correlation lengths drawn with dashed black lines.

For the thermodynamic approach, we quantify the critical fluctuations using the same Ornstein-Zernike approach as applied to the experimental scattering data. While directly fitting the correlation length from simulation scattering patterns is not possible due to finite simulation sizes and the large Q-spacing of the Fourier transformed pair correlation functions at low Q, we can observe the concentration fluctuations in real space. The total density-density correlation function decays as $r^{-1}e^{-r/\xi}$ in classical Ornstein-Zernike theory[62,103,104] for a unary system. For the binary mixture here, where self-association of the extractant drives concentration fluctuations, we consider the long-range decay of DMDBPMA head group correlations defined by the same RDF described above. Figure 7C-D plots these RDFs with fits to $g(r) = Ar^{-1}e^{-r/\xi} + C$, where A and C are constants that are fit and ξ is taken from the experimental fit of the closest corresponding experimental volume fraction. (By fitting C, rather than assuming a value of unity, we allow for deviation to slightly lower values due to finite size effects of the simulation box where local concentration enhancement depletes the observed bulk concentration.) The simulation data are consistent with this form of the long-range decay, particularly at the higher extractant concentrations where the statistical accuracy of the RDF is best. No long-range decay in $g(r)$ is observed for the pure DMDBPMA simulation as there are no concentration fluctuations in the pure phase. We note that the fitted values of the correlation length are sensitive to the range of r values over which the data are fit, and we expect that longer simulation trajectories and larger simulation box sizes would improve the accuracy of fitted correlation lengths. Overall, simulation data suggest that extractant clustering is consistent with critical concentration fluctuations lacking characteristic aggregates sizes.

Conclusions

Organic phase aggregation is an important—yet poorly understood—phenomenon in LLE. While its connection to third phase formation has been implicitly understood in the litera-

ture, we have only recently proposed that the mechanism of aggregation is associated with the liquid-liquid critical point. Here, we demonstrated this explicit relationship by quantifying organic phase structure over a wide composition range for binary extractant/diluent mixtures. We find that structure in these simple binary systems are dominated by critical fluctuations that are characterized by 3D Ising exponents. Molecular dynamics simulations are consistent with this mechanism of extractant aggregation, showing a lack of characteristic aggregate size.

As the complex multicomponent organic phases that we previously studied[63,64] also feature 3D Ising exponents, interpreting structure in organic phases using the theory of critical phenomena is likely generalizable and approachable with simplified model systems. The systems we study here contain no aqueous solutes, such as metals or coextracted acid or water, demonstrating critical fluctuations are fundamental to the extractant/diluent mixture and the same scaling laws can describe structure in both simple and complex organic phases. We find well-known relationships between phase behavior and extractant and diluent molecular structure are the same as for metal- and acid-containing LLE sytems: increasing extractant chain length or decreasing diluent chain length suppresses third phase formation and therefore the critical fluctuations. This suggests that high-throughput screening of compatible extractant/diluent pairs that suppress third phase formation might, to first order, be achievable by considering simplified binary mixtures. This could dramatically simplify experimental testing and computational modeling.

Many studies on organic phase aggregation report small angle scattering patterns that could be consistent with critical fluctuations,[21,23,33,35,37,39,41,42,49,105–113] potentially representing a different or additional mechanism driving aggregation than the formation of water-in-oil reverse micellar nanostructures. The universality of critical phenomena means that critical fluctuations are similar between chemically different systems once each system is scaled to its respective critical temperature, even when the molecular-level interactions driving the phase transition are fundamentally different. The correlation length obtained from the Ornstein-

Zernike equation represents a characteristic length over which the concentration fluctuations decay. As we find a single diverging lengthscale with temperature scaling consistent with the binary 3D Ising model in both simple and complex systems, Lorentzian-shaped low-Q scattering alone cannot be taken as evidence of any particular nanostructure, such as reverse micellization. Future studies should investigate whether structure in more complex systems is dominated by concentration fluctuations of the extractant or the formation of larger, discrete aggregates or some combination of the two. Overall, this study suggests how critical phenomena theory may provide an explicit, quantitative connection between structure and phase behavior under a wide range of solution conditions encountered in LLE.

Acknowledgements

This work was supported by U.S. Department of Energy (DOE), Office of Science, Office of Basic Energy Sciences, Chemical Sciences, Geosciences, and Biosciences Division, Separation Science Program, under Contract DE-AC02-06CH11357 to UChicago Argonne, LLC, Operator of Argonne National Laboratory. This research used resources of beamlines 12-ID-C and 8-ID-I at the Advanced Photon Source, a U.S. DOE Office of Science User Facility, operated for the DOE Office of Science by Argonne National Laboratory under the same contract number. We gratefully acknowledge the computing resources provided on Bebop, a high-performance computing cluster operated by the Laboratory Computing Resource Center at Argonne National Laboratory.

Supporting Information

Sample and simulation compositions, SAXS Ornstein-Zernike fits and comparison between fitting methods are provided in the Supporting Information.

References

(1) Sholl, D. S.; Lively, R. P. Seven chemical separations to change the world. *Nature News* **2016**, *532*, 435.

(2) Cheisson, T.; Schelter, E. J. Rare earth elements: Mendeleev's bane, modern marvels. *Science* **2019**, *363*, 489–493.

(3) Xie, F.; Zhang, T. A.; Dreisinger, D.; Doyle, F. A critical review on solvent extraction of rare earths from aqueous solutions. *Minerals Engineering* **2014**, *56*, 10–28.

(4) Binnemans, K.; Jones, P. T.; Blanpain, B.; Van Gerven, T.; Yang, Y.; Walton, A.; Buchert, M. Recycling of rare earths: a critical review. *Journal of cleaner production* **2013**, *51*, 1–22.

(5) Reddy, M.; Prasada Rao, T.; Damodaran, A. Liquid-liquid extraction processes for the separation and purification of rare earths. *Mineral Procesing and Extractive Metallurgy Review* **1993**, *12*, 91–113.

(6) Hidayah, N. N.; Abidin, S. Z. The evolution of mineral processing in extraction of rare earth elements using liquid-liquid extraction: A review. *Minerals Engineering* **2018**, *121*, 146–157.

(7) Baldwin, A. G.; Ivanov, A. S.; Williams, N. J.; Ellis, R. J.; Moyer, B. A.; Bryantsev, V. S.; Shafer, J. C. Outer-sphere water clusters tune the lanthanide selectivity of diglycolamides. *ACS central science* **2018**, *4*, 739–747.

(8) Stamberga, D.; Healy, M. R.; Bryantsev, V. S.; Albisser, C.; Karslyan, Y.; Reinhart, B.; Paulenova, A.; Foster, M.; Popovs, I.; Lyon, K., et al. Structure activity relationship approach toward the improved separation of rare-earth elements using diglycolamides. *Inorganic Chemistry* **2020**, *59*, 17620–17630.

(9) Liu, T.; Johnson, K. R.; Jansone-Popova, S.; Jiang, D.-e. Advancing Rare-Earth Separation by Machine Learning. *JACS Au* **2022**, *2*, 1428–1434.

(10) Nash, K.; Braley, J. C. *Challenges for actinide separations in advanced nuclear fuel cycles*; American Chemical Society, 2010; Chapter Nuclear Energy and the Environment, pp 19–38.

(11) Servis, A. G.; Servis, M. J.; McCann, K. P.; Jensen, M. P.; Shafer, J. C. Chemical Understanding of Actinide Separations. *Encyclopedia of Inorganic and Bioinorganic Chemistry* **2021**, 1–21.

(12) Charlesworth, P. Separating the Platinum Group Metals by Liquid-Liquid Extraction. *Platinum Metals Review* **1981**, *25*, 106–112.

(13) Chowdhury, A. U.; Lin, L.; Doughty, B. Hydrogen-bond-driven chemical separations: Elucidating the interfacial steps of self-assembly in solvent extraction. *ACS applied materials & interfaces* **2020**, *12*, 32119–32130.

(14) Zemb, T.; Bauer, C.; Bauduin, P.; Belloni, L.; Dejugnat, C.; Diat, O.; Dubois, V.; Dufrêche, J.; Dourdain, S.; Duvail, M.; Larpent, C.; Testard, F.; Pellet-Rostaing, S. Recycling metals by controlled transfer of ionic species between complex fluids: en route to "ienaics". *Colloid. Polym. Sci.* **2015**, *293*, 1–22.

(15) Poirot, R.; Le Goff, X.; Diat, O.; Bourgeois, D.; Meyer, D. Metal recognition driven by weak interactions: A case study in solvent extraction. *ChemPhysChem* **2016**, *17*, 2112–2117.

(16) Knight, A. W.; Qiao, B.; Chiarizia, R.; Ferru, G.; Forbes, T.; Ellis, R. J.; Soderholm, L. Subtle effects of aliphatic alcohol structure on water extraction and solute aggregation in biphasic water/n-dodecane. *Langmuir* **2017**, *33*, 3776–3786.

(17) Špadina, M.; Bohinc, K. Multi-scale modelling of solvent extraction and the choice of reference state: mesoscopic modelling as a bridge between nanoscale and chemical engineering. *Current Opinion in Colloid & Interface Science* **2020**, *46*, 94–113.

(18) Bourgeois, D.; El Maangar, A.; Dourdain, S. Importance of weak interactions in the formulation of organic phases for efficient liquid/liquid extraction of metals. *Current Opinion in Colloid & Interface Science* **2020**, *46*, 36–51.

(19) Erlinger, C.; Gazeau, D.; Zemb, T.; Madic, C.; Lefrancois, L.; Hebrant, M.; Tondre, C. Effect of nitric acid extraction on phase behavior, microstructure and interactions between primary aggregates in the system dimethyldibutyltetradecylmalonamide (DMDBTDMA)/n-dodecane/water: A phase analysis and small angle X-ray scattering (SAXS) characterisation study. *Solvent Extraction and Ion Exchange* **1998**, *16*, 707–738.

(20) Chiarizia, R.; Nash, K.; Jensen, M.; Thiyagarajan, P.; Littrell, K. Application of the Baxter Model for Hard Spheres with Surface Adhesion to SANS Data for the U(VI)-HNO_3, TBP-n-Dodecane System. *Langmuir* **2003**, *19*, 9592–9599.

(21) Nave, S.; Mandin, C.; Martinet, L.; Berthon, L.; Testard, F.; Madic, C.; Zemb, T. Supramolecular organisation of tri-n-butyl phosphate in organic diluent on approaching third phase transition. *Physical Chemistry Chemical Physics* **2004**, *6*, 799–808.

(22) Nave, S.; Modolo, G.; Madic, C.; Testard, F. Aggregation properties of N, N, N', N'-tetraoctyl-3-oxapentanediamide (TODGA) in n-dodecane. *Solvent extraction and ion exchange* **2004**, *22*, 527–551.

(23) Chiarizia, R.; Jensen, M. P.; Rickert, P. G.; Kolarik, Z.; Borkowski, M.; Thiyagarajan, P. Extraction of zirconium nitrate by TBP in n-octane: Influence of cation type on third phase formation according to the "sticky spheres" model. *Langmuir* **2004**, *20*, 10798–10808.

(24) Chiarizia, R.; Jensen, M.; Borkowski, M.; Thiyagarajan, P.; Littrell, K. Interpretation of Third Phase Formation in the Th (IV)–HNO3, TBP–n-Octane System with Baxter's "Sticky Spheres" Model. *Solvent extraction and ion exchange* **2004**, *22*, 325–351.

(25) Jensen, M. P.; Yaita, T.; Chiarizia, R. Reverse-micelle formation in the partitioning of trivalent f-element cations by biphasic systems containing a tetraalkyldiglycolamide. *Langmuir* **2007**, *23*, 4765–4774.

(26) Chiarizia, R.; Briand, A.; Jensen, M.; Thiyagarajan, P. Sans Study of Reverse Micelles Formed upon the Extraction of Inorganic Acids by TBP in n-Octane. *Solvent Extraction and Ion Exchange* **2008**, *26*, 333–359.

(27) Antonio, M.; Chiarizia, R.; Gannaz, B.; Berthon, L.; Zorz, N.; Hill, C.; Cote, G. Aggregation in solvent extraction systems containing a malonamide, a dialkylphosphoric acid and their mixtures. *Separation Science and Technology* **2008**, *43*, 2572–2605.

(28) Testard, F.; Zemb, T.; Bauduin, P.; Berthon, L. *Ion Exchange and Solvent Extraction: A Series of Advances*; CRC Press: Boca Raton, 2009; Vol. 19; Chapter Third-Phase Formation in Liquid/Liquid Extraction: A Colloidal Approach, pp 381–428.

(29) Ellis, R. J.; Anderson, T. L.; Antonio, M. R.; Braatz, A.; Nilsson, M. A SAXS study of aggregation in the synergistic TBP–HDBP solvent extraction system. *The Journal of Physical Chemistry B* **2013**, *117*, 5916–5924.

(30) Verma, P.; Pathak, P.; Mohapatra, P.; Aswal, V.; Sadhu, B.; Sundararajan, M. An insight into third-phase formation during the extraction of thorium nitrate: evidence for aggregate formation from small-angle neutron scattering and validation by computational studies. *The Journal of Physical Chemistry B* **2013**, *117*, 9821–9828.

(31) Verma, P.; Kumari, N.; Pathak, P.; Sadhu, B.; Sundararajan, M.; Aswal, V.; Mohapatra, P. Investigations on preferential Pu (IV) extraction over U (VI) by N, N-

dihexyloctanamide versus tri-n-butyl phosphate: evidence through small angle neutron scattering and DFT studies. *The Journal of Physical Chemistry A* **2014**, *118*, 3996–4004.

(32) Verma, P. K.; Pathak, P. N.; Kumari, N.; Sadhu, B.; Sundararajan, M.; Aswal, V. K.; Mohapatra, P. K. Effect of successive alkylation of N, N-dialkyl amides on the complexation behavior of uranium and thorium: solvent extraction, small angle neutron scattering, and computational studies. *The Journal of Physical Chemistry B* **2014**, *118*, 14388–14396.

(33) Ellis, R. J.; Meridiano, Y.; Muller, J.; Berthon, L.; Guilbaud, P.; Zorz, N.; Antonio, M. R.; Demars, T.; Zemb, T. Complexation-Induced Supramolecular Assembly Drives Metal-Ion Extraction. *Chemistry–A European Journal* **2014**, *20*, 12796–12807.

(34) Chandrasekar, A.; Suresh, A.; Sivaraman, N.; Aswal, V. Trends in small angle neutron scattering of actinide–trialkyl phosphate complexes: a molecular insight into third phase formation. *RSC advances* **2016**, *6*, 92905–92916.

(35) Ferru, G.; Reinhart, B.; Bera, M. K.; Olvera de la Cruz, M.; Qiao, B.; Ellis, R. J. The lanthanide contraction beyond coordination chemistry. *Chemistry–A European Journal* **2016**, *22*, 6899–6904.

(36) Baldwin, A.; Servis, M.; Yang, Y.; Bridges, N.; Wu, D.; Shafer, J. The Structure of Tributyl Phosphate Solutions: Nitric Acid, Uranium (VI), and Zirconium (IV). *Journal of Molecular Liquids* **2017**, *246*, 225–235.

(37) Motokawa, R.; Kobayashi, T.; Endo, H.; Mu, J.; Williams, C. D.; Masters, A. J.; Antonio, M. R.; Heller, W. T.; Nagao, M. A Telescoping View of Solute Architectures in a Complex Fluid System. *ACS central science* **2018**, *5*, 85–96.

(38) Bapat, D. U.; Dalvi, V. H. Molecular Insights into Water Clusters Formed in Tributylphosphate–Di-(2-ethylhexyl) phosphoric Acid Extractant Systems from Ex-

periments and Molecular Dynamics Simulations. *The Journal of Physical Chemistry B* **2019**, *123*, 1618–1635.

(39) Lu, Z.; Dourdain, S.; Pellet-Rostaing, S. Understanding the Effect of the Phase Modifier n-Octanol on Extraction, Aggregation, and Third-Phase Appearance in Solvent Extraction. *Langmuir* **2020**, *36*, 12121–12129.

(40) Artese, A.; Dourdain, S.; Boubals, N.; Dumas, T.; Solari, P. L.; Menut, D.; Berthon, L.; Guilbaud, P.; Pellet-Rostaing, S. Evidence of Supramolecular Origin of Selectivity in Solvent Extraction of Bifunctional Amidophosphonate Extractants with Different Configurations. *Solvent Extraction and Ion Exchange* **2021**, 1–23.

(41) Sarkar, S.; Suresh, A.; Sivaraman, N.; K Aswal, V. Studies on the aggregation behavior of mineral acid and Zr (IV) loaded Tris (2-methylbutyl) phosphate and tri-n-alkyl phosphate systems using small angle neutron scattering. *Separation Science and Technology* **2021**, 1–11.

(42) Dourdain, S.; Špadina, M.; Rey, J.; Bohinc, K.; Pellet-Rostaing, S.; Dufrêche, J.-F.; Zemb, T. How acidity rules synergism and antagonism in liquid–liquid extraction by lipophilic extractants—Part I: Determination of nanostructures and free energies of transfer. *Solvent Extraction and Ion Exchange* **2022**, *40*, 86–105.

(43) Verma, P. K.; Karak, A.; Sahu, P.; Aswal, V. K.; Mahanty, B.; Ali, S. M.; Egberink, R. J.; Huskens, J.; Verboom, W.; Mohapatra, P. K. Aggregation Behavior of Nitrilotriacetamide (NTAmide) Ligands in Thorium (IV) Extraction from Acidic Medium: Small-Angle Neutron Scattering, Fourier Transform Infrared, and Theoretical Studies. *Langmuir* **2022**,

(44) Rao, P.; Kolarik, Z. A Review of Third Phase Formation in Extraction of Actinides by Neutral Organophoshporus Extractants. *Solvent Extraction and Ion Exchange* **1996**, *14*, 955–993.

(45) Durain, J.; Bourgeois, D.; Bertrand, M.; Meyer, D. Comprehensive studies on third phase formation: application to U (VI)/Th (IV) mixtures extracted by TBP in N-dodecane. *Solvent Extraction and Ion Exchange* **2019**, *37*, 328–346.

(46) Cote, G. The supramolecular speciation: a key for improved understanding and modelling of chemical reactivity in complex systems. *Radiochimica Acta* **2003**, *91*, 639–644.

(47) Chiarizia, R.; Jensen, M.; Borkowski, M.; Ferraro, J.; Thiyagarajan, P.; Littrell, K. Third Phase Formation Revisited: The U(VI), HNO_3, TBP, n-Dodecane System. *Solvent Extraction and Ion Exchange* **2003**, *21*, 1–27.

(48) Chiarizia, R.; Jensen, M.; Borkowski, M.; Ferraro, J.; Thiyagarajan, P.; Littrell, K. SANS Study of Third Phase Formation in the U(VI)-HNO_3/TBP/n-Dodecane System. *Separation Science and Technology* **2003**, *38*, 3313–3331.

(49) Ellis, R. J.; Antonio, M. R. Coordination structures and supramolecular architectures in a cerium (III)–malonamide solvent extraction system. *Langmuir* **2012**, *28*, 5987–5998.

(50) Servis, M.; Wu, D.; Braley, J. Network Analysis and Percolation Transition in Hydrogen Bonded Clusters: Nitric Acid and Water Extracted by Tributyl Phosphate. *Physical Chemistry and Chemical Physics* **2017**, *19*, 11326–11339.

(51) Rama Swami, K.; Venkatesan, K.; Antony, M. Aggregation behavior of alkyldiglycolamides in n-dodecane medium during the extraction of Nd (III) and nitric acid. *Industrial & Engineering Chemistry Research* **2018**, *57*, 13490–13497.

(52) Swami, K. R.; Venkatesan, K.; Antony, M. Role of phase modifiers in controlling the third-phase formation during the solvent extraction of trivalent actinides. *Solvent Extraction and Ion Exchange* **2019**, *37*, 500–517.

(53) Sarkar, S.; Suresh, A.; Sivaraman, N.; Aswal, V. K. An insight into third-phase formation in the extraction of thorium nitrate by tris (2-methylbutyl) phosphate and tri-n-alkyl phosphates. *Separation Science and Technology* **2019**, *54*, 970–984.

(54) Sarkar, S.; Ammath, S.; Kirubananthan, S.; Suneesh, A. S. Investigation of the Phase Splitting Behaviour of U (VI) and Th (IV) loaded Trialkyl Phosphate Solvents in the Absence of Aqueous Phase. *ChemistrySelect* **2021**, *6*, 13725–13735.

(55) Dhawa, A.; Rout, A.; Jawahar, N.; Venkatesan, K. A systematic approach for achieving the maximum loading of Eu (III) in TODGA/n-dodecane phase with the aid of TBP phase modifier. *Journal of Molecular Liquids* **2021**, *341*, 117397.

(56) Berthon, L.; Paquet, A.; Saint-Louis, G.; Guilbaud, P. How Phase Modifiers Disrupt Third-phase Formation in Solvent Extraction Solutions. *Solvent Extraction and Ion Exchange* **2021**, *39*, 204–232.

(57) Massey, D.; Masters, A.; Macdonald-Taylor, J.; Woodhead, D.; Taylor, R. Molecular Dynamics Study of the Aggregation Behavior of N, N, N, N-Tetraoctyl Diglycolamide. *The Journal of Physical Chemistry B* **2022**, *126*, 6290–6300.

(58) Lu, Z.; Dourdain, S.; Demé, B.; Dufrêche, J.-F.; Zemb, T.; Pellet-Rostaing, S. Effect of alkyl chain configuration of tertiary amines on uranium extraction and phase stability–Part I: Evaluation of phase stability, extraction, and aggregation properties. *Journal of Molecular Liquids* **2022**, *349*, 118409.

(59) Servis, M. J.; Stephenson, G. Mesostructuring in Liquid–Liquid Extraction Organic Phases Originating from Critical Points. *The Journal of Physical Chemistry Letters* **2021**, *12*, 5807–5812.

(60) Servis, M. J.; Nayak, S.; Seifert, S. The pervasive impact of critical fluctuations in liquid–liquid extraction organic phases. *The Journal of Chemical Physics* **2021**, *155*, 244506.

(61) Servis, M. J.; Piechowicz, M.; Shkrob, I. A.; Soderholm, L.; Clark, A. E. Amphiphile Organization in Organic Solutions: An Alternative Explanation for Small-Angle X-ray Scattering Features in Malonamide/Alkane Mixtures. *The Journal of Physical Chemistry B* **2020**, *124*, 10822–10831.

(62) Stanley, H. E. Introduction to phase transitions and critical phenomena. **1971**,

(63) Sheyfer, D.; Zhang, Q.; Lal, J.; Loeffler, T.; Dufresne, E.; Sandy, A.; Narayanan, S.; Sankaranarayanan, S.; Szczygiel, R.; Maj, P., et al. Nanoscale critical phenomena in a complex fluid studied by x-ray photon correlation spectroscopy. *Phys. Rev. Lett.* **2020**, *125*, 125504.

(64) Sheyfer, D.; Servis, M. J.; Zhang, Q.; Lal, J.; Loeffler, T.; Dufresne, E.; Sandy, A.; Narayanan, S.; Sankaranarayanan, S. K.; Szczygiel, R., et al. Advancing Chemical Separations: Unraveling the Structure and Dynamics of Phase Splitting in Liquid–Liquid Extraction. *The Journal of Physical Chemistry B* **2022**, *126*, 2420–2429.

(65) Chiarizia, R.; Briand, A. Third Phase Formation in the Extraction of Inorganic Acids by TBP in n-Octane. *Solvent Extraction and Ion Exchange* **2007**, *25*, 351–371.

(66) Berthon, L.; Martinet, L.; Testard, F.; Madic, C.; Zemb, T. Solvent penetration and sterical stabilization of reverse aggregates based on the DIAMEX process extracting molecules: Consequences for the third phase formation. *Solvent extraction and ion exchange* **2007**, *25*, 545–576.

(67) Suresh, A.; Srinivasan, T.; Rao, P. V. Parameters influencing third-phase formation in the extraction of Th (NO3) 4 by some trialkyl phosphates. *Solvent Extraction and Ion Exchange* **2009**, *27*, 132–158.

(68) Servis, M. J.; Wu, D. T.; Shafer, J. C.; Clark, A. E. Square supramolecular assemblies of uranyl complexes in organic solvents. *Chemical Communications* **2018**, *1*, 10064–10067.

(69) Spjuth, L.; Liljenzin, J.; Skålberg, M.; Hudson, M.; Chan, G.; Drew, M.; Feaviour, M.; Iveson, P.; Madic, C. Extraction of actinides and lanthanides from nitric acid solution by malonamides. *Radiochimica Acta* **1997**, *78*, 39–46.

(70) Lumetta, G. J.; Rapko, B. M.; Garza, P. A.; Hay, B. P.; Gilbertson, R. D.; Weakley, T. J.; Hutchison, J. E. Deliberate design of ligand architecture yields dramatic enhancement of metal ion affinity. *Journal of the American Chemical Society* **2002**, *124*, 5644–5645.

(71) Geist, A.; Berthon, L.; Charbonnel, M.-C.; Müllich, U. Extraction of nitric acid, Americium (III), Curium (III), and Lanthanides (III) into DMDOHEMA dissolved in kerosene. *Solvent Extraction and Ion Exchange* **2020**, *38*, 681–702.

(72) Seifert, S.; Winans, R. E.; Tiede, D. M.; Thiyagarajan, P. Design and performance of a ASAXS (Anomalous Small Angle X-ray Scattering) instrument at the Advanced Photon Source. *J. Appl. Crystallogr.* **2000**, 782–784.

(73) Dreiss, C. A.; Jack, K. S.; Parker, A. P. On the absolute calibration of bench-top small-angle X-ray scattering instruments: a comparison of different standard methods. *Journal of applied crystallography* **2006**, *39*, 32–38.

(74) Abraham, M.; Murtol, T.; Schulz, R.; Pall, S.; Smith, J.; Hess, B.; Lindhal, E. GROMACS: High performance molecular simulations through multi-level parallelism from laptops to supercomputers. *SoftwareX* **2015**, *1-2*, 19–25.

(75) Martínez, L.; Andrade, R.; Birgin, E.; Martínez, J. PACKMOL: A Package for Building Initial Configurations for Molecular Dynamics Simulations. *J. Comp. Chem.* **2009**, *30*, 2157–2164.

(76) Berendsen, H.; Postma, J.; van Gunsteren, W.; DiNola, A.; Haak, J. Molecular dynamics with coupling to an external bath. *J. Chem. Phys.* **1984**, *81*, 3684.

(77) Hoover, W. Canonical dynamics: Equilibrium phase-space distributions. *Phys. Rev A* **1985**, *31*, 1695–1697.

(78) Hockney, R. W.; Goel, S. P.; Eastwood, J. Quiet High Resolution Computer Models of a Plasma. *J. Comp. Phys.* **1974**, 148–158.

(79) Hess, B.; Bekker, H.; Berendsen, H.; Fraaije, J. LINCS: A constrained solver for molecular simulations. *J. Comput. Chem.* **1997**, *18*, 1463–1472.

(80) Darden, T.; York, D.; Pedersen, L. An N·log(N) method for Ewald sums in large systems. *J. Chem. Phys.* **1993**, 10089–10092.

(81) Lohithakshan, K.; Aswal, V.; Aggarwal, S. Studies on the third-phase formation in DHDECMP/dodecane/HNO3. *Radiochimica Acta* **2011**, *99*, 179–186.

(82) Bauduin, P.; Testard, F.; Berthon, L.; Zemb, T. Relation between the hydrophile/hydrophobe ratio of malonamide extractants and the stability of the organic phase: Investigation at high extractant concentrations. *Physical Chemistry Chemical Physics* **2007**, *9*, 3776–3785.

(83) Dozol, H.; Berthon, C. Characterisation of the supramolecular structure of malonamides by application of pulsed field gradients in NMR spectroscopy. *Physical Chemistry Chemical Physics* **2007**, *9*, 5162–5170.

(84) Fisher, M. E. Correlation functions and the critical region of simple fluids. *Journal of Mathematical Physics* **1964**, *5*, 944–962.

(85) Fisher, M. E.; Burford, R. J. Theory of critical-point scattering and correlations. I. The Ising model. *Physical Review* **1967**, *156*, 583.

(86) Xu, L.; Kumar, P.; Buldyrev, S. V.; Chen, S.-H.; Poole, P. H.; Sciortino, F.; Stanley, H. E. Relation between the Widom line and the dynamic crossover in systems

with a liquid–liquid phase transition. *Proceedings of the National Academy of Sciences* **2005**, *102*, 16558–16562.

(87) Brazhkin, V.; Fomin, Y. D.; Ryzhov, V.; Tareyeva, E.; Tsiok, E. True Widom line for a square-well system. *Physical Review E* **2014**, *89*, 042136.

(88) Ni, Y.; Skinner, J. Evidence for a liquid-liquid critical point in supercooled water within the E3B3 model and a possible interpretation of the kink in the homogeneous nucleation line. *The Journal of Chemical Physics* **2016**, *144*, 214501.

(89) Raju, M.; Banuti, D. T.; Ma, P. C.; Ihme, M. Widom lines in binary mixtures of supercritical fluids. *Scientific reports* **2017**, *7*, 1–10.

(90) Kim, K. H.; Späh, A.; Pathak, H.; Perakis, F.; Mariedahl, D.; Amann-Winkel, K.; Sellberg, J. A.; Lee, J. H.; Kim, S.; Park, J., et al. Maxima in the thermodynamic response and correlation functions of deeply supercooled water. *Science* **2017**, *358*, 1589–1593.

(91) Hestand, N. J.; Skinner, J. Perspective: Crossing the Widom line in no man's land: Experiments, simulations, and the location of the liquid-liquid critical point in supercooled water. *The Journal of Chemical Physics* **2018**, *149*, 140901.

(92) Strong, S. E.; Shi, L.; Skinner, J. Percolation in supercritical water: Do the Widom and percolation lines coincide? *The Journal of chemical physics* **2018**, *149*, 084504.

(93) Regueira, T.; Yan, W.; Stenby, E. H. Densities of the binary systems n-hexane+ n-decane and n-hexane+ n-hexadecane up to 60 MPa and 463 K. *Journal of Chemical & Engineering Data* **2015**, *60*, 3631–3645.

(94) Mhanna, R.; Lefort, R.; Noirez, L.; Morineau, D. Microstructure and concentration fluctuations in alcohol–Toluene and alcohol-Cyclohexane binary liquids: A small angle neutron scattering study. *J. Mol. Liq.* **2016**, *218*, 198–207.

(95) Shibuta, S.; Imamura, H.; Nishikawa, K.; Morita, T. Fluctuational parameters based on the Bhatia–Thornton theory for supercritical solutions: Application to a supercritical aqueous solution of n-pentane. *Chemical Physics* **2017**, *487*, 30–36.

(96) Stephenson, G. B.; Warburton, W. K.; Haller, W.; Bienenstock, A. Real-time small-angle x-ray scattering study of the early stage of phase separation in the SiO 2-BaO-K 2 O system. *Physical Review B* **1991**, *43*, 13417.

(97) Morita, T.; Kusano, K.; Ochiai, H.; Saitow, K.-i.; Nishikawa, K. Study of inhomogeneity of supercritical water by small-angle x-ray scattering. *The Journal of Chemical Physics* **2000**, *112*, 4203–4211.

(98) Nishikawa, K.; Morita, T. Inhomogeneity of molecular distribution in supercritical fluids. *Chemical Physics Letters* **2000**, *316*, 238–242.

(99) Sengers, J. V.; Shanks, J. G. Experimental critical-exponent values for fluids. *Journal of Statistical Physics* **2009**, *137*, 857–877.

(100) Servis, M. J.; Piechowicz, M.; Soderholm, L. Impact of Water Extraction on Malonamide Aggregation: A Molecular Dynamics and Graph Theoretic Approach. *The Journal of Physical Chemistry B* **2021**, *125*, 6629–6638.

(101) Stauffer, D.; Aharony, A. *Introduction to percolation theory*; CRC press, 2018.

(102) Campi, X.; Krivine, H.; Sator, N. Percolation line of self-bound clusters in supercritical fluids. *Physica A* **2001**, *296*, 24–30.

(103) Wikfeldt, K. T.; Huang, C.; Nilsson, A.; Pettersson, L. G. Enhanced small-angle scattering connected to the Widom line in simulations of supercooled water. *The Journal of chemical physics* **2011**, *134*, 214506.

(104) Nilsson, A.; Huang, C.; Pettersson, L. G. Fluctuations in ambient water. *Journal of Molecular Liquids* **2012**, *176*, 2–16.

(105) Plaue, J.; Gelis, A.; Czerwinski, K.; Thiyagarajan, P.; Chiarizia, R. Small-Angle Neutron Scattering Study of Plutonium Third Phase Formation in 30% TBP/HNO3/Alkane Diluent Systems. *Solvent extraction and ion exchange* **2006**, *24*, 283–298.

(106) Chiarizia, R.; Stepinski, D.; Antonio, M. SANS study of HCl extraction by selected neutral organophosphorus compounds in n-octane. *Separation Science and Technology* **2010**, *45*, 1668–1678.

(107) Ellis, R. J.; Meridiano, Y.; Chiarizia, R.; Berthon, L.; Muller, J.; Couston, L.; Antonio, M. R. Periodic behavior of lanthanide coordination within reverse micelles. *Chemistry–A European Journal* **2013**, *19*, 2663–2675.

(108) Qiao, B.; Demars, T.; Olvera de la Cruz, M.; Ellis, R. J. How hydrogen bonds affect the growth of reverse micelles around coordinating metal ions. *The journal of physical chemistry letters* **2014**, *5*, 1440–1444.

(109) Déjugnat, C.; Dourdain, S.; Dubois, V.; Berthon, L.; Pellet-Rostaing, S.; Dufrêche, J.-F.; Zemb, T. Reverse aggregate nucleation induced by acids in liquid–liquid extraction processes. *Phys. Chem. Chem. Phys.* **2014**, *16*, 7339–7349.

(110) Qiao, B.; Ferru, G.; Olvera de la Cruz, M.; Ellis, R. J. Molecular origins of mesoscale ordering in a metalloamphiphile phase. *ACS central science* **2015**, *1*, 493–503.

(111) Swami, K. R.; Venkatesan, K.; Selvan, B. R.; Hase, D. V.; Jayaram, R. Investigations on the unusual aggregation behaviour of tetra (2-ethyhexyl) diglycolamide in n-dodecane medium upon gamma irradiation. *Journal of Molecular Liquids* **2020**, *319*, 114177.

(112) Moreno Martinez, D.; Acher, E.; Vatin, M.; Dourdain, S.; Guillaumont, D.; Guilbaud, P. Aggregation of Bifunctional Extractants Used for Uranium (VI) Separation. *The Journal of Physical Chemistry B* **2021**, *125*, 10759–10771.

(113) El Maangar, A.; Prévost, S.; Dourdain, S.; Zemb, T. Molecular mechanisms induced by phase modifiers used in hydrometallurgy: consequences on transfer efficiency and process safety. *Comptes Rendus. Chimie* **2022**, *25*, 341–360.

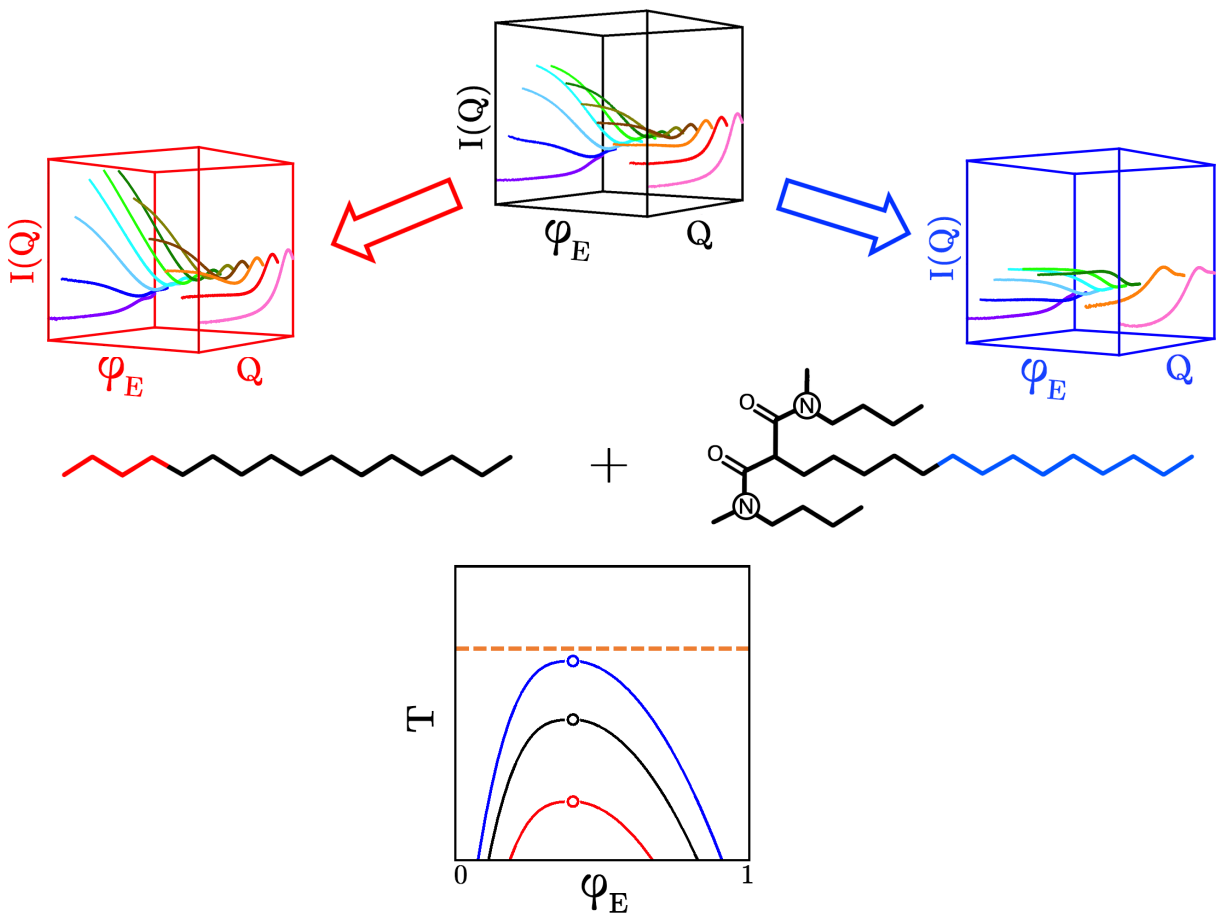

TOC image.